Core Loss Analysis for the Planar Switched Reluctance Motor

J. F. Pan[1], F. J. Meng[1], and Norbert C. Cheung[2]

[1]Shenzhen Key Laboratory of Electromagnetic Control, Shenzhen University, Shenzhen 518060, China
[2]Department of Electrical Engineering, The Hong Kong Polytechnic University, Hong Kong

Core loss is one of the key factors for performance evaluation of switched reluctance machines. In this paper, core loss analysis of the planar switched reluctance motor (PSRM) is calculated based on the 3-D time-stepping finite element methods. The numerical analysis for the computation of the core loss is discussed, also its transient and average core loss in the mover and the stator are calculated. The corresponding experiments of measurement loss for a PSRM prototype are conducted and the results validate the accuracy from the numerical analysis. It can be concluded that core loss dominates around the corner of the mover and stator cores.

Index Terms— **Core loss, FEM, numerical analysis, PSRM.**

I. Introduction

PLANAR motors are suitable for 2-D, direct-drive applications in the industry, such as electronic component insertion, integrated circuit packaging, and precision watch assembly, and so forth. Based on the machine construction, planar motor can be classified as permanent magnet (PM) type or switched reluctance type [1]–[4]. In [1], characteristic analysis of a long-stroke synchronous PM planar motor is discussed by employing the finite element method (FEM). The performance analysis of the PM-type planar motor characteristics such as detent force, flux density, and so forth is investigated in [2] with machine optimization scheme.

The effects of eddy current in permanent magnets from the permanent magnet motors are analyzed in [5] and [6]. It has been verified that the losses in the PMs inevitably increase the working temperature, degrade the performance of the PM materials, and decrease the efficiency of the PM machines. The common procedure that describes core loss analysis for rotary electrical machines based on the FEMs can be found in [7]. Three core loss models from the traditional technique model, the advanced technique model, and the hybrid model are discussed and compared. Core loss estimation of rotary switched reluctance machines is analyzed in [8] and [9]. A loss measurement method based on FEM and the experimental technique to calculate core loss rates in high-speed rotary switched reluctance machines is discussed in [8]. The flux waveforms in different parts of the switched reluctance motor are evaluated using 2-D finite element transient analysis and the improved Steinmetz Equation is applied for core loss calculation [9].

However, few papers have focused on the loss study of planar machines, especially on the planar switched reluctance motors (PSRMs). In this paper, the calculation of core loss is performed based on the 3-D time-stepping FEM and derivation of average loss by electrical and mechanical parameters from the PSRM prototype is also discussed. The simulation results match closely with those from the experiment. The results from the loss study of the PSRM provide considerable insights to the design and optimization for this type of machine.

Manuscript received June 18, 2013; revised August 19, 2013; accepted October 7, 2013. Date of current version February 21, 2014. Corresponding author: N. C. Cheung (e-mail: norbert.cheung@polyu.edu.hk).

Color versions of one or more of the figures in this paper are available online at http://ieeexplore.ieee.org.

Digital Object Identifier 10.1109/TMAG.2013.2285377

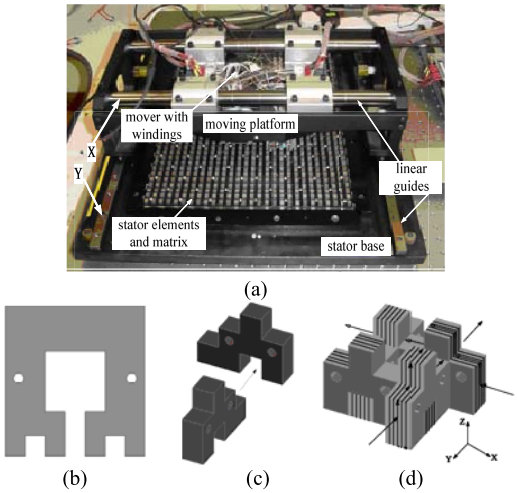

Fig. 1. (a) Machine prototype, (b) mover lamination, (c) formation of stator matrix, and (d) stator block and flux circulation in two axes.

II. Machine Structure

The planar machine can be regarded as the combination of two linear switched reluctance motors with two perpendicular movement of axis maintained at the same level [4]. Fig. 1(a) shows the PSRM prototype. The moving platform consists of two sets of three-phase movers with windings, and the mover lamination can be found in Fig. 1(b). Each set of three-phase movers and windings is responsible for one direction of motion, so the two sets provide two axes of motion as a 2-D, direct-drive manner. The stator contains multiple laminated silicon steel blocks held by epoxy glues. To reduce eddy current loss, the stator matrix is assembled by inserting one leg of the stator component to the leg hole of another one, as shown in Fig. 1(c). The other pair can be connected in the same manner as the previous one. Then, the stator block can be constructed, as shown in Fig. 1(d), with perpendicular flux circulation. When the winding of any phase is excited, the stator blocks with laminations along that axis are responsible for the establishment of a flux path. To ensure 2-D flux circulation perpendicularly, the bricks topology of the stator matrix realize flux circulation through the contact regions between stator component legs with epoxy glues [10]. Table I lists the major specifications of the machine. For each axis of movement, the machine applies the asymmetric H-bridge drive topology with rated dc supply set as 40 V. The power

TABLE I
MAJOR MACHINE SPECIFICATIONS

Parameter	Value
Material model of silicon steel plates	50W1300
Lamination thickness	0.5 mm
Stacking factor	0.95
Mover mass (X)	8.75 kg
Mover mass (Y)	15 kg
No. of turns per phase	160
Air gap length	0.55 mm
Conductivity	2×10^6 S/m
Phase resistance	1.5 Ω
Rated DC link voltage	40 V

transistors from the drive circuit are controlled in a pulse width modulation manner for correct current chopping [4].

III. THEORETICAL ANALYSIS

A. Theoretical Analysis

Core loss P_v in the PSRM consists of eddy current loss P_c, hysteresis loss P_h, and excess loss P_e [7], [11]. Core loss can be represented from (1) as [12]

$$P_v = P_h + P_c + P_e. \tag{1}$$

In the time domain, the instantaneous hysteresis loss can be computed as [13]

$$P_h(t) = H_{\text{irr}} \frac{dB}{dt} \tag{2}$$

where H_{irr} is the irreversible component of the magnetic field and B is the amplitude of flux density of the PSRM.

The instantaneous eddy current loss and instantaneous excess loss in the time domain can be expressed as (3) and (4), respectively

$$P_c(t) = \frac{1}{2\pi^2} K_c \left(\frac{dB}{dt}\right)^2 \tag{3}$$

$$P_e(t) = \frac{1}{C_e} K_e \left|\frac{dB}{dt}\right|^{1.5} \tag{4}$$

where K_c and K_e are the eddy current core loss coefficient and the excess loss coefficient, respectively. The core loss coefficients such as K_c and K_e are defined by electrical properties of steel material and can be found from the manufacturer data by least square fitting [14]. From the PSRM prototype, $K_c = 1.402$, $K_e = 12.175$ and C_e can be calculated from numerical integration with $C_e = 8.763363$ [12].

For the 3-D time-stepping FEM calculation, (2)–(4) can be modified as [12]

$$P_h(t) = \left\{ \left|H_x \frac{dB_x}{dt}\right|^{2/\beta} + \left|H_y \frac{dB_y}{dt}\right|^{2/\beta} + \left|H_z \frac{dB_z}{dt}\right|^{2/\beta} \right\}^{\beta/2} \tag{5}$$

$$P_c(t) = \frac{1}{2\pi^2} K_c \left\{ \left(\frac{dB_x}{dt}\right)^2 + \left(\frac{dB_y}{dt}\right)^2 + \left(\frac{dB_z}{dt}\right)^2 \right\} \tag{6}$$

$$P_e(t) = \frac{1}{C_e} K_e \left\{ \left(\frac{dB_x}{dt}\right)^2 + \left(\frac{dB_y}{dt}\right)^2 + \left(\frac{dB_z}{dt}\right)^2 \right\}^{0.75}. \tag{7}$$

For $\beta = 2$, which is an empirical parameter obtained from the experimental measurement under sinusoidal excitation [12].

TABLE II
DISCRETIZATION DATA

Parameter	Value		
Number of mover elements	356707		
Number of stator elements	624581		
Speed	0.05 m/s	0.08 m/s	0.1 m /s
Calculation time	45h 50m 28s	47h 45m 36s	47h 12m 48s

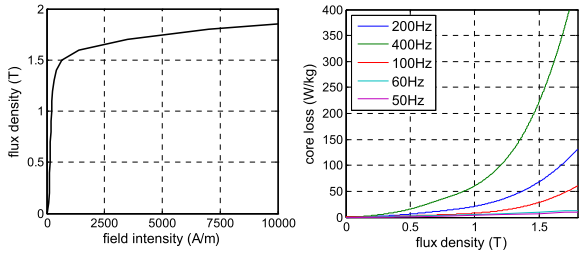

Fig. 2. Material characteristics. (a) B–H and (b) B–P curves.

B. 3-D Time-Stepping FEM

The 3-D time-stepping FEM is applied to calculate the distribution of the copper loss in the coil windings and the core loss in the silicon steel plates of the mover and the stator using ANSOFT Maxwell 3-D. Since the 3-D time-stepping FEM needs more time steps and long computation time, the mesh quality directly affects the accuracy of the calculation. The 3-D finite element discretization meshes of the mover and stator finite elements are shown in Table II.

The magnetization characteristics of B–H curve and electrical steel material characteristics of B–P curve for the PSRM are shown in Fig. 2(a) and (b), respectively. The core loss data of the material are input for calculation of the machine core loss based on the 3-D time-stepping FEM. Parameters of K_c and K_e can also be derived from the core loss data as well.

IV. RESULTS AND DISCUSSION

A. Simulation Results from FEM

Since each phase from the two axes owns the same dimensions and ratings, any one mover with windings and the stator can be constructed as the 3-D FEM model for simulation. The drive employs the typical asymmetric H-bridge with dc link voltage of 40 V [11]. Fig. 3(a) shows the drive topology for any direction of movement. For example, according to the current command of winding A from x-axis of movement, transistors T_1 and T_2 will be turned on for proper current circulation. If the transistors are turned off, the energy stored in the winding A will keep the current in the same direction until it is depleted. Diodes D_1 and D_2 become forward biased leading to recharging of the source. The magnetic flux distribution contour at the unaligned position for the mover relative to the stator can be found in Fig. 3(b). It can be observed from Fig. 3(c) that the flux distributes within the short magnetic path among the mover, the stator area and the air gap region between them. Most of the flux lines penetrate through both the mover/stator teeth and air gaps. Flux lines

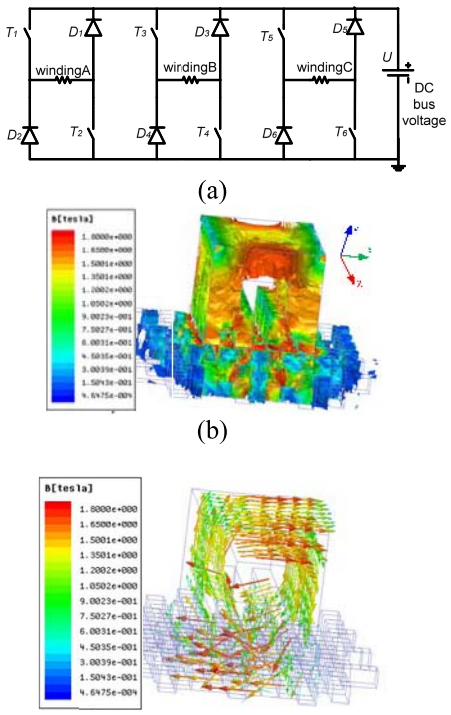

Fig. 3. (a) Drive topology, (b) 3-D magnetic flux contour, and (c) flux distribution.

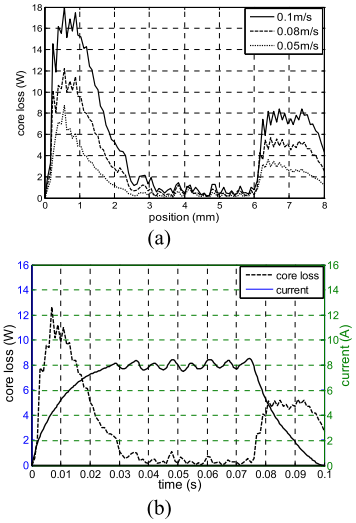

Fig. 4. Dynamic core loss profiles (a) and current waveform (0.08 m/s) (b)

distribute mostly in the mover and the stator teeth, compared with mover and stator yokes. Therefore, there is a higher tendency of saturation from the teeth.

The dynamic core loss profiles of any one phase without load according to different speed levels can be derived, as shown in Fig. 4(a). The core loss profile together with current waveform at speed level of 0.08 m/s can be found in Fig. 4(b). It is clear that transient core loss increases with speed. It can also be observed that two peaks appear around the fully unaligned positions (0 mm) and the fully aligned positions (6 mm). The peak values at the unaligned positions are higher, since the change rate of the phase current is high and the air gap reluctance varies, as shown in Fig. 4(b).

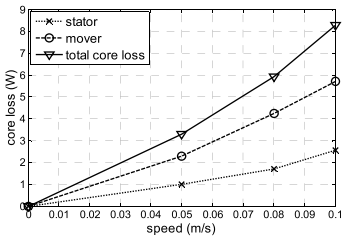

Fig. 5. Average core loss of the PSRM.

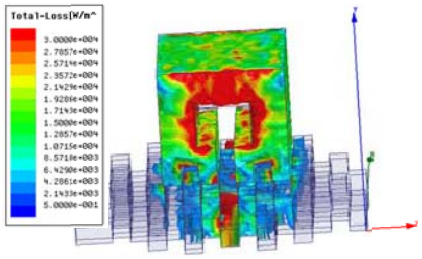

Fig. 6. 3-D FEM results of total loss distribution.

As shown in Fig. 5, the average core loss of the PSRM is separated into stator, mover, and total core loss, respectively. The values are calculated according to different speed levels. It can be concluded that the average core loss increase with speed as well. The mover core loss is much higher than that of the stator and the value of mover core loss is 0.6941, 0.7143, and 0.6892 to that of the total core loss at different speed levels, respectively.

Fig. 6 shows the total core loss distribution in the stator and mover for one of the phases. It is clear that the loss in the mover core is higher than that in the stator core. It can also been found that total core loss around the corner of the mover and stator cores are larger than other parts. To reduce the core loss of the laminations, one method is to use arc corner laminations instead of vertical corner laminations, and results show that using arc corner will decrease almost 2.5% of core loss compared with vertical corner laminations [15].

B. Experimental Results

The experiment is performed under the dSPACE DS1104 controller card installed on the personal computer. Three commercial current drivers are employed for inner current regulation and they are fast enough to meet the requirements for position control of the linear switched reluctance actuator that drives the PSRM. A force gauge and a linear optical encoder with resolution of 1 μm are mounted on the translator of the linear actuator. The overall experimental setup can be found, as shown in Fig. 7.

The input power of any one phase from the PSRM can be determined as the average of the product of input current from the driver and the dc link voltage, whereas the output power is obtained by multiplying the speed and the constant load of the motor. The copper loss is calculated by multiplying the resistance of the phase winding and the square of current flowing through the phase.

Core loss can be obtained by subtracting the known losses from the measured losses [11]. Therefore, the experimental core loss can be represented as follows:

$$P_{vm} = P_{\text{in}} - P_{\text{out}} - P_{cu} - P_{fw} - P_{st} \tag{8}$$

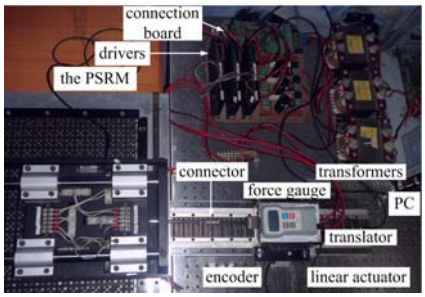

Fig. 7. Experimental setup.

TABLE III
EXPERIMENTAL RESULTS OF CORE LOSS FROM ANY AXIS

Parameter	Speed value (m/s)		
	0.05	0.08	0.1
Measured copper loss (W)	10.150	11.539	15.870
Friction and wingding loss (W)	0.6220	1.0330	1.1260
Measured core loss (W)	4.155	5.458	8.554
Simulated core loss (W)	3.288	5.928	8.273
Pvm/Pin (%)	27.70	30.12	32.93

where P_{vm} is the measured core loss, P_{in} is the input power, P_{out} is the output power, P_{cu} is the copper loss, and P_{fw} is the friction and windage loss. P_{st} is the stray load loss, predicted by the fixed-value method [16] as 0.0906 W, which is 0.5% of the input power.

Friction and windage loss are independent on the load of the machine. However, they are dependent on the speed of the motor as well as on the air gap length and the stack length of the PSRM. In addition, the normal force makes a significant contribution to the friction and windage loss [11]. Since it is difficult to mount any sensor among the air gaps for accurate measurement of the normal force, FEM is used to calculate the effect of different current excitation levels on normal force F_n at different positions. Coefficient of the kinetic friction of the longitudinal direction $\mu_x = 0.0339$ is obtained by measuring the friction and windage force F_{fw} of the PSRM, driven by the linear actuator. Coefficient of kinetic friction of the perpendicular direction $\mu_y = 0.0532$ can be evaluated.

The friction and windage loss are measured as the average product of normal force times coefficient of kinetic friction multiplied by the constant speed. The measured core loss values are listed in Table III at the operation speeds of 0.05, 0.08, and 0.1 m/s, respectively. It can be concluded that the core loss percentage to the total input power of 27.70%, 30.12%, and 32.93% can be derived, respectively.

As the speed increases, the copper loss and the core loss will also increase and they accounts for ∼95% of the input power. It is also shown that the rate of the core loss to the total input power increases as the rate of the copper loss to the total input power is reduced.

V. CONCLUSION

In this paper, the core loss of the PSRM prototype has been investigated using 3-D time-stepping FEM and results are verified by the experiment. The experimental results correspond to the simulation data. Results show that the density of core loss dominates in the vertical corner and teeth of the mover and stator and it account for ∼30% of the input power without load. Since core loss is one of the significant factors of the total loss in a PSRM, it is essential for the design and optimization of efficient PSRMs.

ACKNOWLEDGMENT

The authors would like to thank the National Natural Science Foundation of China and Guangdong Natural Science Foundation for sponsoring of research projects under the code 51007059 and S2011010001208. They would also like to thank the Shenzhen government and Hong Kong Polytechnic University Central Research Grant under the code of JCYJ20130329144017199, A-PJ21, and G-YX2Q for support.

REFERENCES

[1] L. Zhang, B. Kou, H. Zhang, and S. Guo, "Characteristic analysis of a long-stroke synchronous permanent magnet planar motor," *IEEE Trans. Magn.*, vol. 48, no. 11, pp. 4658–4661, Nov. 2012.

[2] W. Min, M. Zhang, Y. Zhu, F. Liu, G. Duan, J. Hu, *et al.*, "Analysis and design of novel overlapping ironless windings for planar motors," *IEEE Trans. Magn.*, vol. 47, no. 11, pp. 4635–4642, Nov. 2011.

[3] J. Cao, Y. Zhu, W. Yin, and W. Xu, "Electromagnetic forces acting on the planar armature of a core-type synchronous permanent-magnet planar motor," *IEEE Trans. Magn.*, vol. 45, no. 8, pp. 3145–3150, Aug. 2009.

[4] J. F. Pan, N. C. Cheung, W. C. Gan, and S. W. Zhao, "A novel planar switched reluctance motor for industrial applications," *IEEE Trans. Magn.*, vol. 42, no. 10, pp. 2836–2839, Oct. 2006.

[5] Y. Kawase, T. Ota, and H. Fukunaga, "3-D eddy current analysis in permanent magnet of interior permanent magnet motors," *IEEE Trans. Magn.*, vol. 36, no. 4, pp. 1863–1866, Jul. 2000.

[6] Y. Amara, J. Wang, and D. Howe, "Analytical prediction of eddy-current loss in modular tubular permanent-magnet machines," *IEEE Trans. Energy Convers.*, vol. 20, no. 4, pp. 761–770, Dec. 2005.

[7] E. Dlala, "Comparison of models for estimating magnetic core losses in electrical machines using the finite-element method," *IEEE Trans. Magn.*, vol. 45, no. 2, pp. 716–725, Feb. 2009.

[8] B. Minh and U. Schaefer, "Core losses measurement technique for high frequency and flux density of switched reluctance machines," in *Proc. IEEE 20th ICEM*, Sep. 2012, pp. 1619–1624.

[9] B. Ganji, J. Faiz, K. Kasper, C. E. Carstensen, and R. W. De Doncker, "Core loss model based on finite-element method for switched reluctance motors," *IET Electr. Power Appl.*, vol. 4, no. 7, pp. 569–577, Aug. 2010.

[10] J. Pan, N. C. Cheung, and J. Yang, "High-precision position control of a novel planar switched reluctance motor," *IEEE Trans. Ind. Electron.*, vol. 52, no. 6, pp. 1644–1652, Dec. 2005.

[11] J. T. Charton, J. Corda, J. M. Stephenson, and S. P. Randall, "Dynamic modeling of switched reluctance machines with iron losses and phase interactions," *IET Electr. Power Appl.*, vol. 153, no. 3, pp. 327–336, May 2006.

[12] D. Lin, P. Zhou, W. N. Fu, Z. Badics, and Z. J. Cendes, "A dynamic core loss model for soft ferromagnetic and power ferrite materials in transient finite element analysis," *IEEE Trans. Magn.*, vol. 40, no. 2, pp. 1318–1321, Mar. 2004.

[13] D. Lin, P. Zhou, Q. M. Chen, N. Lambert, and Z. J. Cendes, "The effects of steel lamination core losses on 3D transient magnetic fields," *IEEE Trans. Magn.*, vol. 46, no. 8, pp. 3539–3542, Aug. 2010.

[14] V. Raulin, A. Radun, and I. Husain, "Modeling of losses in switched reluctance machines," *IEEE Trans. Ind. Appl.*, vol. 40, no. 6, pp. 1560–1569, Nov./Dec. 2004.

[15] W. Min, J. T. Chen, Z. Q. Zhu, Y. Zhu, M. Zhang, and G. H. Duan, "Optimization and comparison of novel E-core and C-core linear switched flux PM machines," *IEEE Trans. Magn.*, vol. 47, no. 8, pp. 2134–2141, Aug. 2011.

[16] G. Tong and M. Zhai, "Study on stray load losses algorithm based on EH-star method," in *Proc. Int. Conf. WAC*, Jun. 2012, pp. 1–4.